

# Characterization of Cr–ZrO<sub>2</sub> composite coatings electrodeposited from Cr(III) bath

G. Bikulčius<sup>1</sup>,

A. Češūnienė<sup>1\*</sup>,

A. Selskienė<sup>1</sup>,

A. Grigucevičienė<sup>1</sup>,

V. Jasulaitienė<sup>1</sup>,

M. Ger<sup>2</sup>

<sup>1</sup> Institute of Chemistry,  
Center for Physical Sciences and Technology,  
Saulėtekio Ave. 3, 10257 Vilnius, Lithuania

<sup>2</sup> Proteomics Center,  
Institute of Biochemistry,  
Life Sciences Center,  
Vilnius University, Saulėtekio Ave. 7,  
10257 Vilnius, Lithuania

The aim of this work was to incorporate ZrO<sub>2</sub> particles into a Cr matrix within the research work aimed at obtaining metal matrix composite coatings (Cr–ZrO<sub>2</sub>) under direct current and to evaluate their protective properties. A Cr–ZrO<sub>2</sub> composite coating was deposited from an electrolyte based on trivalent chromium sulphate with formate-urea as a complexing agent containing various concentrations of ZrO<sub>2</sub>. Cross-section investigations have revealed that ZrO<sub>2</sub> particles incorporated into the Cr coating are uniformly distributed. The results indicate that ZrO<sub>2</sub> particles influence the microhardness, morphology and corrosion behaviour of Cr–ZrO<sub>2</sub> composite coatings obtained from the Cr(III) bath.

**Keywords:** zirconium, electrodeposited films, SEM, XPS, EIS, interfaces

## INTRODUCTION

Hard chromium electrodeposition is extensively used in modern industry as it provides good corrosion and wear resistances of the coatings obtained. Commonly, chromium coatings are deposited from hazardous hexavalent chromium baths. In view of a very high toxicity of Cr(VI) compounds, the development of an alternative hexavalent chromium plating process is urgently needed. According to the EU Regulation (EC) No. 1907/2006 (“REACH”) the use of chromium trioxide baths for functional and decorative chromium plating will be forbidden or severely limited after 1 September 2017.

Among many potential alternatives, trivalent chromium (Cr(III)) plating is considered as a very promising technology to replace conventional hexavalent Cr plating. Inasmuch as Cr coatings deposited in Cr(III) baths do not feature such good properties as Cr coatings deposited in Cr(VI) baths, efforts have been made to improve them by various methods.

Electrochemical codeposition of inert particles in a metal matrix is a suitable technique to produce composite materials with new exploitation properties. Different hard dispersion phases distinguish themselves for different electrical conductivity and surface charge, therefore, to incorporate one or another hard disperse phase into a metallic matrix, specific deposition conditions are required [1].

One of popular ceramic particles is ZrO<sub>2</sub>. It is known [2, 3] that ZrO<sub>2</sub> has many superior properties, such as high

\* Corresponding author. Email: asta.cesuniene@ftmc.lt

melting temperature (2700°C), low thermal conductivity and high chemical stability, thus Ni–ZrO<sub>2</sub> composite coatings provide excellent resistance to hot corrosion and oxidation. ZrO<sub>2</sub> particles are successfully incorporated into matrices such as Ni, [3–5], Cu [6], Zn [7] and Co [8]. In all cases ZrO<sub>2</sub> improves both mechanical (microhardness, wear resistance) and corrosion resistance properties of the coatings.

Attempts have been made to electrochemically incorporate ZrO<sub>2</sub> disperse particles into Cr(VI) coatings. It has been known [9] that an attempt was made to electrochemically incorporate ZrO<sub>2</sub> into the Cr(VI) coating in order to enhance the corrosion resistance of the coating. However, according to the Surviliene et al. ZrO<sub>2</sub> particles were deposited only on the surface of the coating. Hashimoto et al. [10] incorporated ZrO<sub>2</sub> into the Cr(VI) coating applying the impulse electrochemical deposition method. This made it possible to enhance coating microhardness and corrosion resistance. However, they did not present any evidence that ZrO<sub>2</sub> was incorporated into the bulk of the matrix. Lakra et al. [11] tried to incorporate ZrO<sub>2</sub> into the Cr(VI) coating by applying both constant and impulse current. They obtained Cr–ZrO<sub>2</sub> composites in both cases, but the composites formed under the influence of impulse current possessed better mechanical properties. However, they did not present information on ZrO<sub>2</sub> incorporation into the Cr matrix. Attempts have long been made to incorporate disperse particles such as SiC [12], Al<sub>2</sub>O<sub>3</sub> [13, 14] and carbon-nanotube [15] into the Cr coating deposited in the Cr(III) bath. However, more or less reliable data on the incorporation of disperse particles into the Cr matrix are not available.

The aim of this work was to form a Cr(III)–ZrO<sub>2</sub> composite in an environment-friendly Cr(III) bath under the conditions of constant current and to study the incorporation of ZrO<sub>2</sub> disperse particles into the Cr matrix, the elemental composition of the Cr–ZrO<sub>2</sub> composite, surface microhardness (HV), surface morphology (SEM, XPS) and corrosion resistance (OCP, Tafel and EIS).

## EXPERIMENTAL

Cr–ZrO<sub>2</sub> composite coatings were deposited from the Cr(III) bath containing Cr<sub>2</sub>(SO<sub>4</sub>)<sub>3</sub>·6H<sub>2</sub>O (150 g l<sup>-1</sup>), H<sub>3</sub>BO<sub>3</sub> (30 g l<sup>-1</sup>), Na<sub>2</sub>SO<sub>4</sub> (60 g l<sup>-1</sup>), Al<sub>2</sub>(SO<sub>4</sub>)<sub>3</sub>·18H<sub>2</sub>O (120 g l<sup>-1</sup>), NaF (20 g l<sup>-1</sup>), HCOONa (27 g l<sup>-1</sup>), NH<sub>2</sub>COONH<sub>2</sub> (g l<sup>-1</sup>) under a 30 l h<sup>-1</sup> agitation flow of compressed air with a direct current density of 0.2 A cm<sup>-2</sup> and pH 2.0 at 20°C. This trivalent chromium bath composition was taken from literature [16]. The maximum size of ZrO<sub>2</sub> particles was about 0.5–2.5 μm. The solution was agitated prior to electrolysis for 4 h. All solutions were prepared using distilled water and analytical grade chemicals (manufacturer AppliChem GmbH). The Cu substrate (1.5 Si, 98.5 Cu wt.%) was mechanically degreased by grinding with 600-grit SiC paper, washed in distilled water and then electropolished in a commercial degreasing solution (H<sub>3</sub>PO<sub>4</sub> 350 ml (conc ≥87.5%); izobutil-alkohol 90 ml)

at 20°C under a current density of 0.05 A cm<sup>-2</sup> for 3 min, using the substrate as an anode. A pure Cu plate was used as a cathode. After that the samples were washed with distilled water, soaked in a hot 20 vol.% HCl solution, washed again with distilled water and then immediately placed in the plating bath. Electrolyte pH was adjusted to 2.0 using H<sub>2</sub>SO<sub>4</sub> or KOH. A bath of a volume of 1 l with vertical Pt with an area of 2 × 4 cm<sup>2</sup> anodes and a cathode between them was maintained at a constant temperature. The cathode (Cu substrate) and anode were disposed within the bath at a distance of 25 mm. Chromium deposits were obtained on both sides of the specimen (one side area was 1 cm<sup>2</sup>). The cathode/anode ratio was 1:4. Chromium electroplating was performed without separation of the anodic and cathodic compartments. The deposition thickness was about 5 μm.

A Helios NanoLab 650 DualBeam workstation (FEI) was used for the surface of chromium coatings (SEM) and the elemental composition was studied employing an energy dispersive spectrometer with an Xmax 20 mm<sup>2</sup> EDS detector (Oxford Instruments).

Measurements of the deposit thickness were done by using the weight and cross-section methods. The samples were weighed before and after the electrodeposition. Several specimens were analysed by producing localized cross sections by focused Ga ion beaming with a Helios NanoLab 650. Before the formation of cross-sections on the specimens a protective platinum (Pt) overcoat ~1 μm thick was deposited by electron and ion beams. Such a thick Pt overcoat layer helps avoid the Ga ion damage to the edge regions of the studied coating. Then the specimen was placed under Ga ion beam exposure perpendicularly to the surface until the necessary depth was reached. The SEM images of the cross section were studied at an accelerating voltage of 3 kV and a current of 6.3 pA.

Microhardness tests were performed on the surface of the coatings using a PTM-3 (Russia) set-up at a load of 50 g. The values of HV are the average of five indentations.

XPS measurements were carried out to obtain information on the elemental chemical states and surface composition of six samples of powders on an upgraded Vacuum Generator (VG) ESCALAB MKII spectrometer fitted with a new XR4 twin anode. The non-monochromatised MgK<sub>α</sub> X-ray source operated at  $h\nu = 1253.6$  eV with 300 W power (20 mA/15 kV) and the pressure in the analysis chamber was lower than  $5 \times 10^{-7}$  Pa during the spectral acquisition. The spectra were acquired with an electron analyser pass energy of 20 eV for narrow scans and a resolution of 0.05 eV and with a pass energy of 100 eV for survey spectra. All spectra were recorded at a 90° take-off angle and calibrated from the hydrocarbon contamination using the C 1s peak at 284.6 eV. The spectra calibration, processing and fitting routines were done using the Avantage software (5.962) provided by Thermo VG Scientific. Core level peaks of Cr<sub>2p</sub> were analysed using a nonlinear Shirley-type

background and the calculation of the elemental composition was performed on the basis of Scofield's relative sensitivity factors. The samples were etched in the preparation chamber by ionized argon at a vacuum of  $5 \cdot 10^{-4}$  Pa. XPS analyses are given for coatings at the etching time of 2 min. The sputter rate for  $\text{Cr}^0$  is 14 nm/min under  $100 \mu\text{A}/\text{cm}^2$  current.

All electrochemical experiments (OCP, potentiodynamic polarization and EIS) measurements were performed using a potentiostat/galvanostat/FRA Zahner Zennium. Measurements were performed at  $20 \pm 1^\circ\text{C}$  in a naturally aerated 3.5% NaCl solution. Reagents of analytical grade and deionized water were used to prepare the solution. A platinum plate of  $4 \text{ cm}^2$  area served as a counter electrode and the saturated Ag/AgCl/KCl electrode was used as the reference and all potential values in the text refer to this electrode. The working electrode (a Cu plate with the deposited chromium coating) was mounted in a special holder and placed into a three-electrode electrochemical glass cell with a volume of  $100 \text{ cm}^3$ . The area of the working electrode surface exposed to the electrolyte was  $0.5 \text{ cm}^2$ . The stationary polarization curves were recorded under a potentiodynamic mode at a potential scan rate of  $1 \text{ mV/s}$ . The EIS spectra were recorded under an open circuit potential in a potentiostatic mode with the potential amplitude of  $\pm 10 \text{ mV}$ . The frequency range from 20 KHz to 0.01 Hz was employed. The electrochemical measurements started after 60 min of the electrode exposure to the NaCl solution. The EIS data analysis and simulation were performed using the authorized ZSimpWin™ software. It should be mentioned that before simulations the consistency of ex-

perimental impedance data sets was verified by the Kramers–Kronig relationship test.

## RESULTS AND DISCUSSION

### Effect on $\text{ZrO}_2$ incorporation and surface microhardness

The effect of  $\text{ZrO}_2$  concentration in the Cr(III) bath on the  $\text{ZrO}_2$  content in the Cr– $\text{ZrO}_2$  composite is shown in Fig. 1. With an increase in the  $\text{ZrO}_2$  concentration in the Cr(III) electrolyte from 2 to  $6 \text{ g l}^{-1}$ , the Zr concentration in the Cr matrix increases only slightly. A further increase in the  $\text{ZrO}_2$  concentration in the Cr electrolyte leads to an increase in the concentration of Zr incorporated into the Cr matrix from 2.3 to 4.0 wt.%. Thus, the  $\text{ZrO}_2$  content in the Cr– $\text{ZrO}_2$  deposit increased 2.2 times after the  $\text{ZrO}_2$  concentration in the Cr bath with a formate–urea complex had been increased five times.

It is of interest to compare the results obtained by us with those obtained by other authors. Having no examples of Cr (III) with  $\text{ZrO}_2$ , let us compare  $\text{ZrO}_2$  incorporation into the Ni coating. It is known [17] that nano- and submicro-scaled  $\text{ZrO}_2$  particles may be incorporated into the Ni matrix from a Watts bath employing electrochemical plating. She et al. have reported higher (9 wt%) incorporation of 200 nm size  $\text{ZrO}_2$  particles into the Ni matrix compared to 40 nm size particles (3 wt%). In our case the incorporation of micro  $\text{ZrO}_2$  particles into the Cr matrix reached 6 wt.%. Huang et al. reported [18] that an increase in the concentration of 40 nm size  $\text{ZrO}_2$  particles in the Ni bath from 4 to

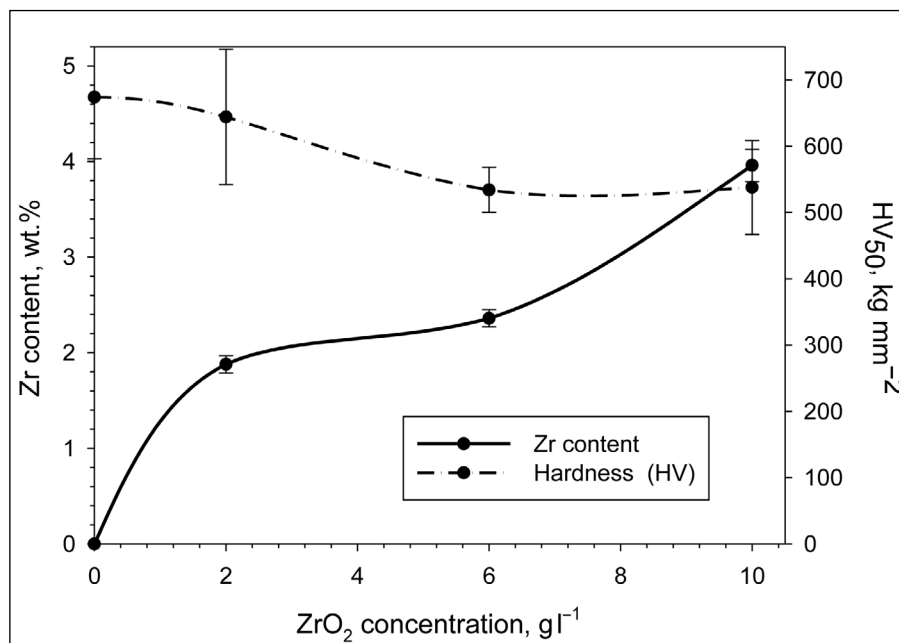


**Fig. 1.** Dependence of the weight percentage of  $\text{ZrO}_2$  incorporated into the Cr matrix and the surface microhardness (HV) on the concentration of  $\text{ZrO}_2$  in the Cr(III) bath

20%, that is fivefold, results only in a 1.6 times higher  $ZrO_2$  content in the Ni- $ZrO_2$  composite.

The effect of  $ZrO_2$  concentration in the Cr(III)g bath on the surface microhardness (HV) of Cr- $ZrO_2$  composite coating is shown in Fig. 1. HV tends to decrease as the  $ZrO_2$  concentration in the Cr(III)<sub>fu</sub> electrolyte increases from 0 to 10 g l<sup>-1</sup>, whereas the concentration of  $ZrO_2$  both in the Ni matrix [4] and Cu matrix [6] enhances the HV of Ni- $ZrO_2$  and Cu- $ZrO_2$  composites. Thus, at a glance a somewhat strange behaviour of HV of the Cr- $ZrO_2$  coating can be

explained through the differences in the microhardness of the matrix and  $ZrO_2$ . It is known [19] that the Vickers microhardness of  $ZrO_2$  (monoclinic) is about 622 kg mm<sup>-2</sup> (6.1 GPa). Hence it is obvious that the higher concentration of  $ZrO_2$  in the composite Cr- $ZrO_2$  coating is the lower its HV will be, as the Cr coating HV itself is about 680 kg mm<sup>-2</sup>.

#### Morphology of Cr- $ZrO_2$ composite coatings

Figure 2 shows the surface morphology of Cr- $ZrO_2$  composite coatings deposited in the electrolyte with different  $ZrO_2$

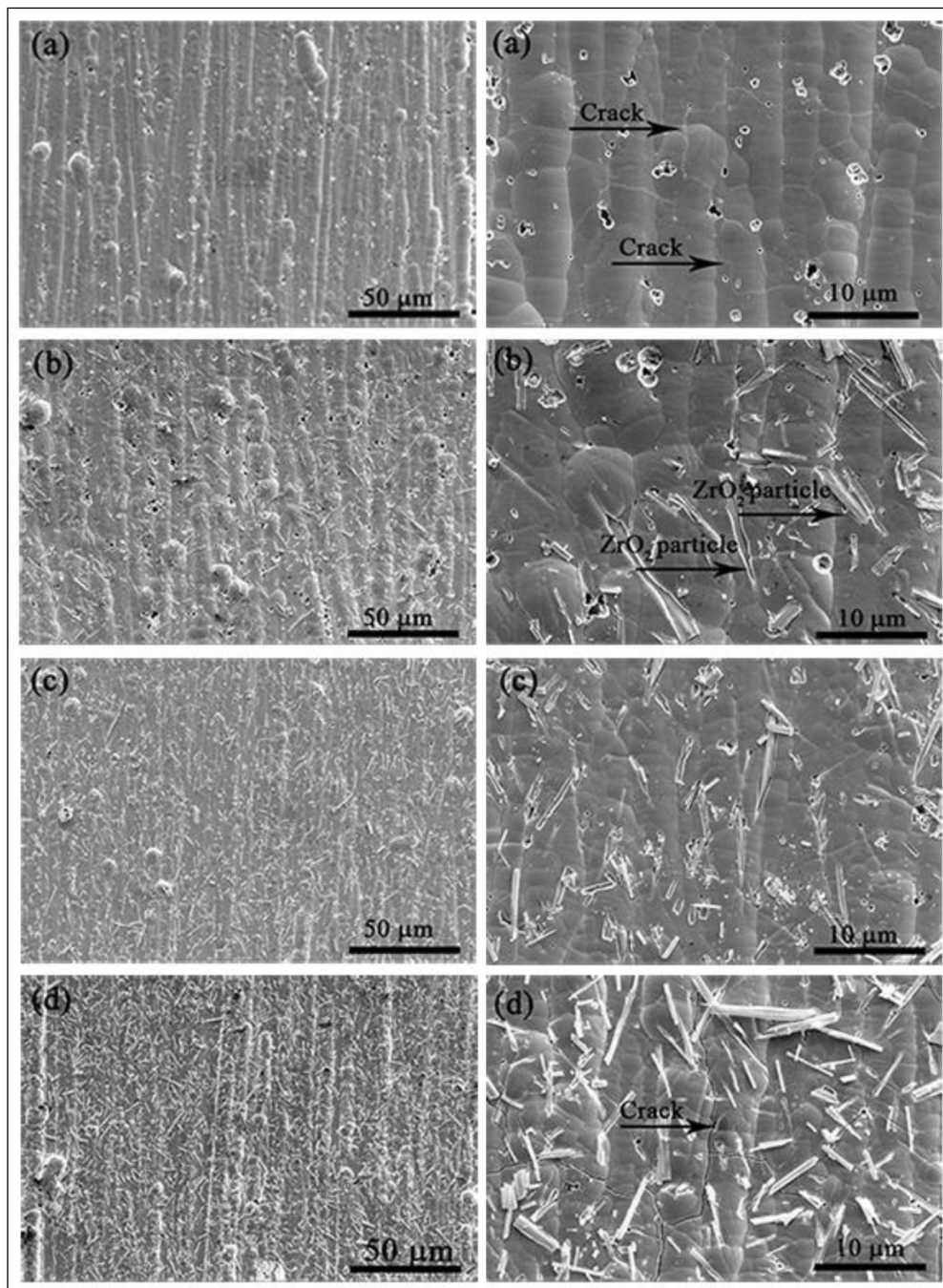


**Fig. 2.** SEM images of the Cr- $ZrO_2$  composite coatings surfaces as deposited at different  $ZrO_2$  concentration in the Cr(III) bath (g l<sup>-1</sup>): 0 (a), 2 (b), 6 (c) and 10 (d)

concentrations. As can be seen from Fig. 2, the Cr coating without  $ZrO_2$  is porous (Fig. 2a) and cracked (Fig. 2a'). After the addition of  $2 \text{ g l}^{-1} ZrO_2$  to the Cr bath the number of pores seen on the surface of the Cr coating remains nearly the same (Fig. 2b), but the coating cracking degree markedly diminishes (Fig. 2b'). After the  $ZrO_2$  concentration had been increased up to  $6 \text{ g l}^{-1}$ , the number of pores diminished nearly by half (Fig. 3c), while cracks nearly disappeared (Fig. 2c'). When the  $ZrO_2$  concentration in the Cr bath is  $10 \text{ g l}^{-1}$ , the Cr coating becomes less porous (Fig. 2d), while cracks completely disappear (Fig. 2d').

### Cross-section

Figure 3 shows the coating cross-section, element mapping image and thickness data of the Cr– $ZrO_2$  composite coating deposited in the Cr(III) bath containing  $10 \text{ g l}^{-1} ZrO_2$ . It is seen from Fig. 3a that the micron-sized particles of  $ZrO_2$  are incorporated into the Cr matrix and distributed non-uniformly in the body of the composite coating. EDS maps of Cr, Cu and Zr distribution in the Cr– $ZrO_2$  composite coating indicate the presence of

$ZrO_2$  (Fig. 3a, d). The thickness of Cr– $ZrO_2$  composite coatings is characterized by high uniformity (Fig. 3e).

### XPS

The XPS analysis was performed to examine the elemental composition of the top layer (in 28 nm depth) of the Cr coating (Fig. 4a) and to determine the valence states of elements, which indicated the presence of  $Cr_2p_3$  (574.82 eV),  $O1s$  (530.75 eV),  $N1s$  (397.29 eV) and  $C1s$  (282.48 eV). The chemical states were identified by comparison of the photoelectron binding energies (BE) with those obtained from the literature [20, 21].

The analysis of the data obtained from Fig. 4a shows that the spectra of  $Cr_2p_3$  can be convoluted into the  $Cr_2p_{3/2}$  spectrum (Fig. 4b), which involves the  $Cr^0$ ,  $Cr_2O_3$ ,  $CrO_2$  and  $CrO_4^{2-}$  spectra. The proportion of  $Cr^0$  ( $p_{Cr^0}$ ) equal to 0.22 in the total quantity of the elemental Cr was calculated upon integrating of the area under the spectrum of every compound ( $Cr^0_{area} = a$ ;  $Cr_2O_3_{area} = b$ ;  $CrO_2_{area} = c$ ;  $CrO_4^{2-}_{area} = d$  and unknown  $_{area} = e$ ), according to Eq. (1):

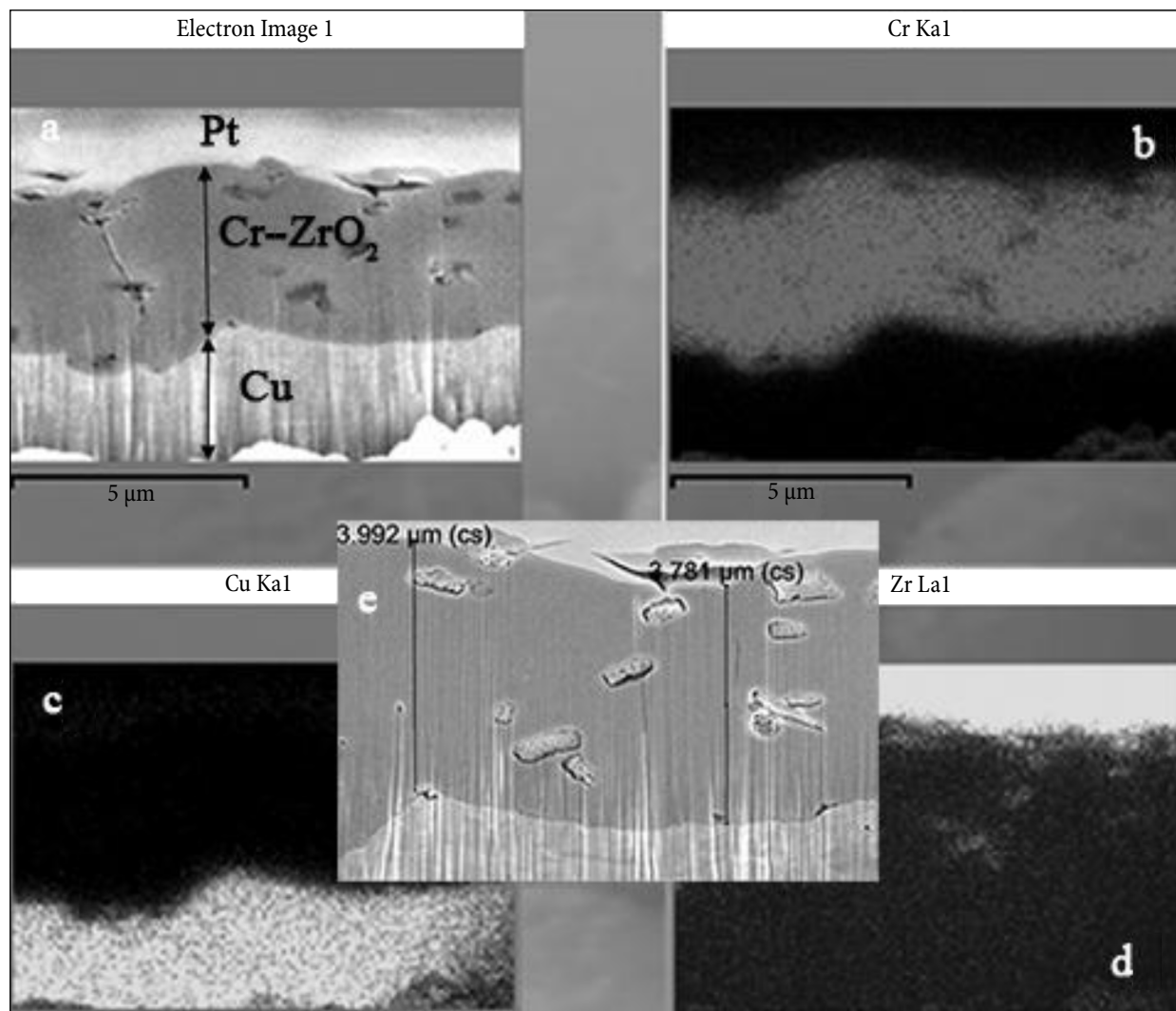


**Fig. 3.** SEM images of the Cr– $ZrO_2$  composite coating deposited in the Cr(III) bath containing  $10 \text{ g l}^{-1} ZrO_2$ : cross-section (a), elements distribution maps of Cr (b), Cu (c), Zr (d) and thickness of composite coating (e)

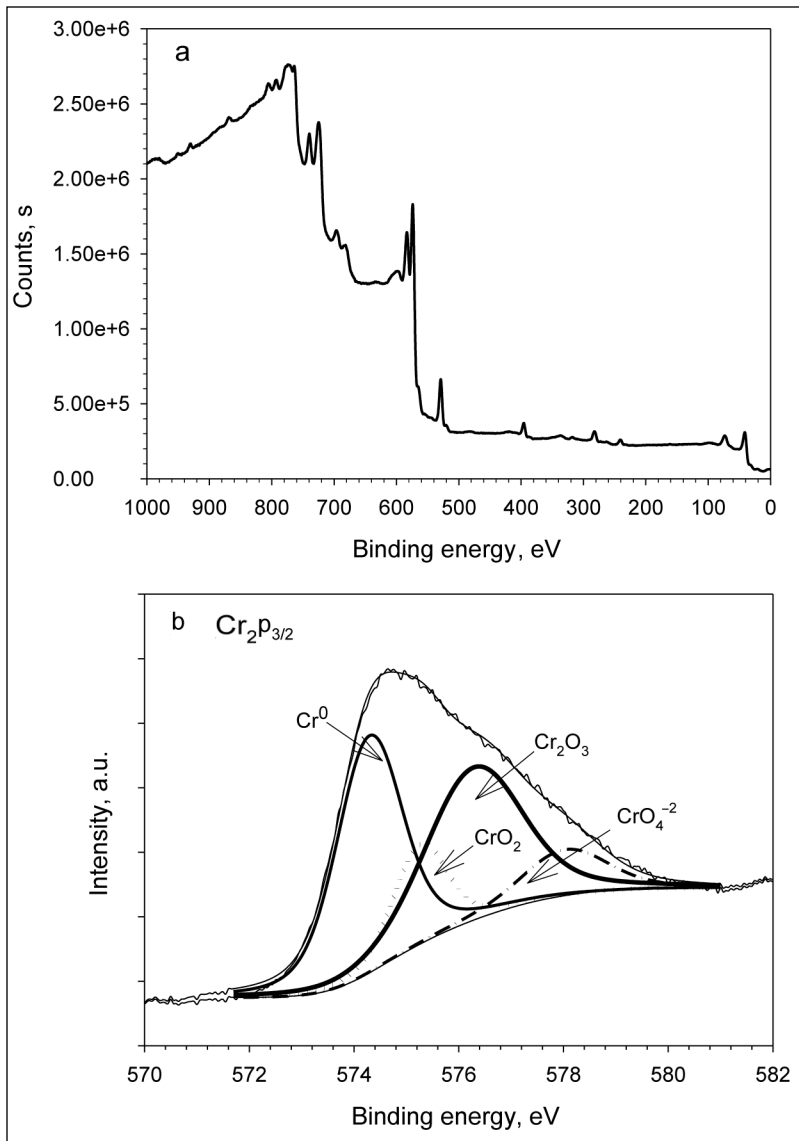


**Fig. 4.** XPS spectra: (a) overview, (b)  $\text{Cr}_{2p}$  spectra of the Cr coating recorded after 2 min sputtering

$$\rho_{\text{Cr}^0} = \frac{a}{b + c + d + e} \quad (1)$$

Employing the Elemental ID and Quantification data, the calculated  $\text{Cr}^0$  quantity in the coating would be equal to 9.33 at.% ( $42.43 \text{ at.}\% \times 0.22 = 9.33 \text{ at.}\%$ ). It is obvious that this is a very approximate evaluation of metallic  $\text{Cr}^0$ , inasmuch as along with the mentioned above compounds there also exist Cr carbides [22].

### OCP

The corrosion behaviour of the electrodeposited Cr and Cr +  $\text{ZrO}_2$  coatings was studied in a 3.5% NaCl solution under conditions of naturally aerated media. The open circuit potential ( $E_{\text{ocp}}$ ) provides information on the electrochemical stability of the coatings in a specific solution [22]. The value of  $E_{\text{ocp}}$  depends on the ratio of the anodic and cathodic reactions rate and varies as the coating develops on the substrate surface. Dependencies of the  $E_{\text{ocp}}$  vs exposure time of

Cr and Cr +  $\text{ZrO}_2$  coatings are shown in Fig. 5. It can be seen that the addition of  $\text{ZrO}_2$  particles to the Cr coating shifted the initial  $E_{\text{ocp}}$  value from  $-0.036 \text{ V}$  for pure Cr to  $\sim -0.302 \text{ V}$  for Cr +  $2 \text{ g l}^{-1} \text{ZrO}_2$ ,  $\sim -0.323 \text{ V}$  for Cr +  $6 \text{ g l}^{-1} \text{ZrO}_2$  and  $\sim -0.322 \text{ V}$  for Cr +  $10 \text{ g l}^{-1} \text{ZrO}_2$  coatings. In the case of pure Cr, at the beginning of immersion, the  $E_{\text{ocp}}$  value decreased due to the formation of chromium oxide, which reduced the rate of anodic dissolution of Cr and the availability of cathodic sites for the oxygen reduction. The potential in  $\sim 8 \text{ min}$  tended to become a relatively stable value of about  $-0.127 \text{ V}$  which indicates the equilibrium of surface reactions. The opposite behaviour was observed for the Cr +  $2 \text{ g l}^{-1} \text{ZrO}_2$  coating: as the duration of coating exposure to NaCl increased,  $E_{\text{ocp}}$  shifted to more positive values, which means surface passivation. The quasi-stationary state of the electrode was achieved after  $\sim 35 \text{ min}$  of exposure. The character of the  $E_{\text{ocp}}$  variations of Cr +  $6 \text{ g l}^{-1} \text{ZrO}_2$  and Cr +  $10 \text{ g l}^{-1} \text{ZrO}_2$  electrodes was similar to that of pure Cr:  $E_{\text{ocp}}$  decreased with immersion time and reached relatively stable values of  $\sim -0.379 \text{ V}$  and  $\sim -0.392 \text{ V}$ , respectively. The last values indicate more corrosion activity of

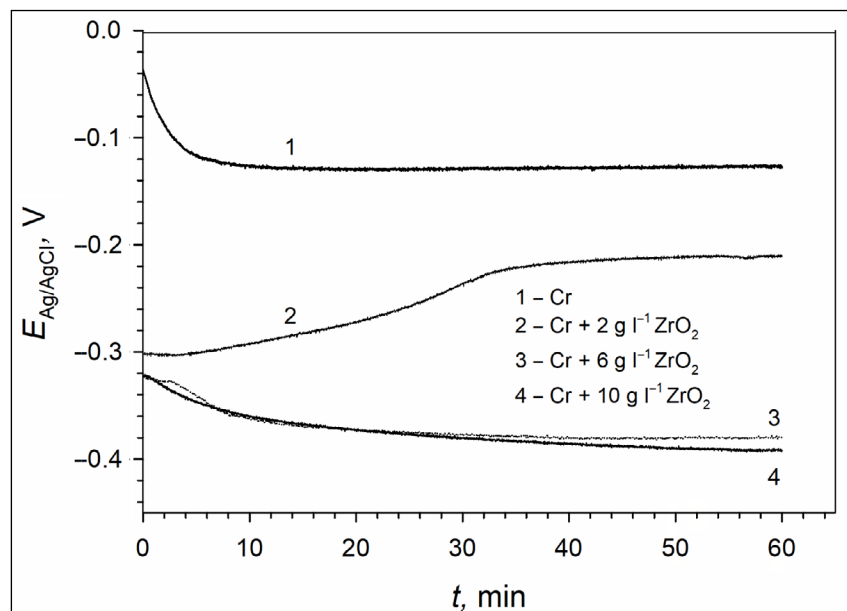


Fig. 5. Dependence of  $E_{\text{ox}}$  of deposited Cr in 3.5% NaCl on the  $\text{ZrO}_2$  content in the coating

Cr + 6 g l<sup>-1</sup>  $\text{ZrO}_2$  and Cr + 10 g l<sup>-1</sup>  $\text{ZrO}_2$  electrodes as compared to those of pure Cr and Cr + 2 g l<sup>-1</sup>  $\text{ZrO}_2$ .

#### Potentiodynamic polarization tests

Corrosion activity of the deposited Cr and Cr +  $\text{ZrO}_2$  coatings was also evaluated by potentiodynamic polarisation measurements in a 3.5% NaCl solution (Fig. 6). Anodic and cathodic curves (Tafel plots) were recorded after the quasi-steady state had been reached (Fig. 5). It can be seen that the addition of  $\text{ZrO}_2$  particles to the chromium solution did not influence the

shape of Tafel curves. Clear Tafel regions (linear parts of  $\lg j$ - $E$  dependences at polarization  $\Delta E > 30$ –60 mV) are expressed on both the cathodic and anodic curves. The corrosion current densities ( $j_{\text{corr}}$ ) of the electrodes were determined by the extrapolating Tafel regions to the corresponding corrosion potentials ( $E_{\text{corr}}$ ). The determined values of  $E_{\text{corr}}$ ,  $j_{\text{corr}}$  and the anodic and cathodic Tafel slopes ( $b_a$  and  $b_c$ , respectively) are presented in Table 1. As can be seen, the  $E_{\text{corr}}$  value for the Cr coating was more positive compared to that of Cr +  $\text{ZrO}_2$  coatings. Higher  $b_a$  and  $b_c$  slopes indicated possible changes in the electrode

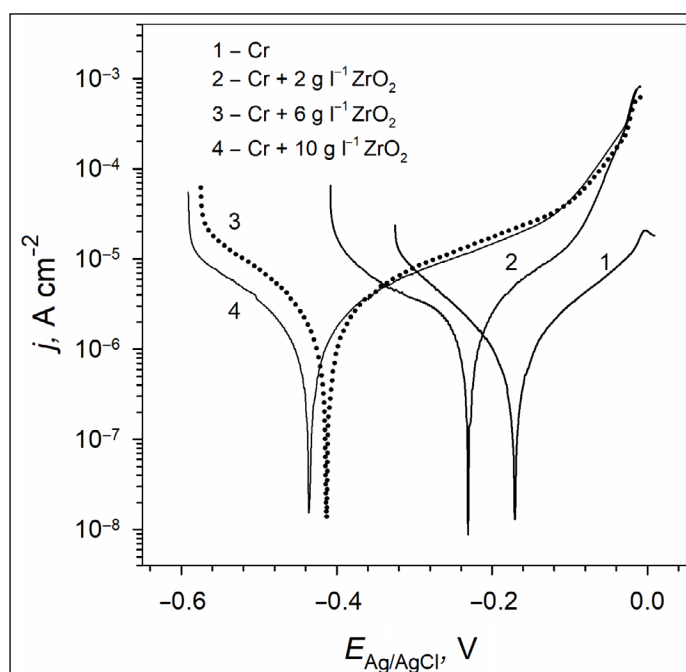


Fig. 6. Potentiodynamic polarization curves of the deposited Cr (1) and Cr- $\text{ZrO}_2$  coatings (2–4) in 3.5% NaCl

Table 1. Corrosion parameters obtained from the polarization studies in 3.5% NaCl

Sample	$E_{\text{corr}}$ , mV	$b_c$ , mV	$b_a$ , mV	$j_{\text{corr}}$ , $\mu\text{A cm}^{-2}$
Cr	-177	-133	146	0.45
Cr + 2 g l <sup>-1</sup> ZrO <sub>2</sub>	-231	-268	153	0.98
Cr + 6 g l <sup>-1</sup> ZrO <sub>2</sub>	-416	-156	206	1.09
Cr + 10 g l <sup>-1</sup> ZrO <sub>2</sub>	-436	-172	198	0.83

reaction mechanisms. The determined  $j_{\text{corr}}$  for the Cr coating was  $\sim 0.45 \mu\text{A cm}^{-2}$  as compared to  $\sim 0.98 \mu\text{A cm}^{-2}$  for Cr + 2 g l<sup>-1</sup> ZrO<sub>2</sub>,  $\sim 1.09 \mu\text{A cm}^{-2}$  for Cr + 6 g l<sup>-1</sup> ZrO<sub>2</sub> and  $\sim 0.83 \mu\text{A cm}^{-2}$  for Cr + 10 g l<sup>-1</sup> ZrO<sub>2</sub>, respectively. It could be concluded that the introduction of ZrO<sub>2</sub> particles into the chromium coating led to an increase in corrosion rates, which depended on the content of ZrO<sub>2</sub> particles.

### Tests of electrochemical impedance spectra

To evaluate the corrosion characteristics of deposited Cr and Cr + ZrO<sub>2</sub> coatings at their respective open circuit potentials, the EIS spectra in 3.5% NaCl were recorded. The experimentally measured and fitted impedance data of the electrodes are presented as Bode plots in Fig. 7. For accurate simulation of the corrosion process the number of capacitive loops

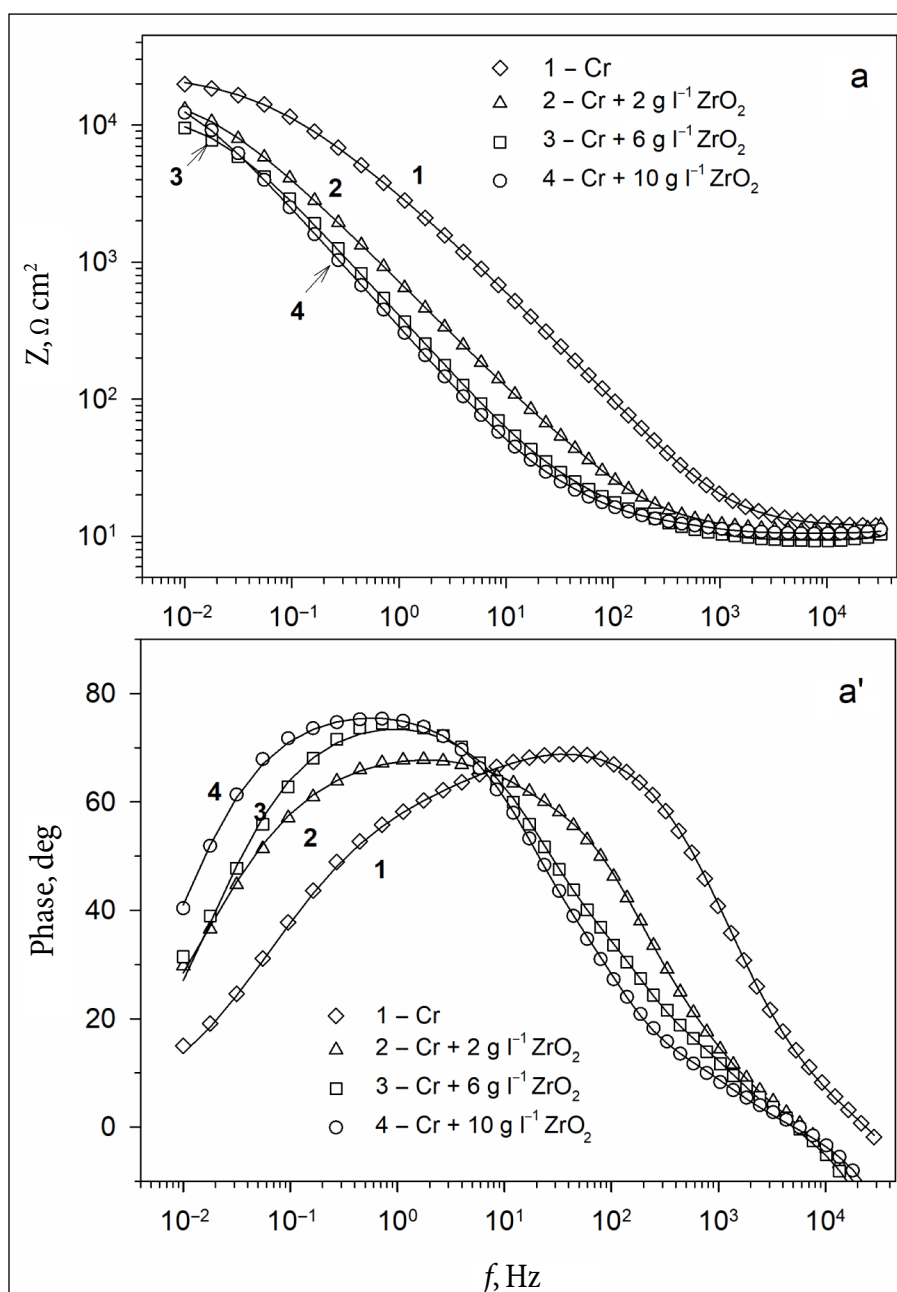


Fig. 7. Bode plots of the deposited Cr (1) and Cr-ZrO<sub>2</sub> coatings (2-4) after 60 min immersion in 3.5% NaCl. The symbols represent the experimental data and the lines are the fitting results obtained assuming an equivalent circuit

(time constants) were identified by Voight circuits according to the procedure proposed by Agarwal et al. [24]. As was determined, the measured impedance spectra of pure Cr and as-deposited Cr + ZrO<sub>2</sub> coatings exhibit one capacitive loop in the medium frequencies range ~ (1–10 kHz) and one capacitive loop in the low frequency domain. Both impedance and phase angle of the electrode spectra depended on the composition of the coating. A simultaneous shift of the capacitive loop in the low frequency range and the increase in phase shift values were observed. The electrodes with ZrO<sub>2</sub> particles exhibited lower polarisation resistances ( $R_p$ ) compared to pure chromium. The  $R_p$  values of deposited chromium coatings determined by the extrapolation of the respective impedance ( $Z$ ) spectrum from a low frequency range to a zero frequency  $Z_{\phi \rightarrow 0}$  were as follows:  $\approx 19.8 \text{ k}\Omega \text{ cm}^2$  for Cr,  $\approx 13 \text{ k}\Omega \text{ cm}^2$  for Cr + 2 g l<sup>-1</sup> ZrO<sub>2</sub>,  $\approx 9.5 \text{ k}\Omega \text{ cm}^2$  for Cr + 6 g l<sup>-1</sup> ZrO<sub>2</sub> and  $\approx 12.2 \text{ k}\Omega \text{ cm}^2$  for Cr + 10 g l<sup>-1</sup> ZrO<sub>2</sub>. It can be seen that the introduction of ZrO<sub>2</sub> particles into the Cr coating led to a decrease in the corresponding electrode  $R_p$  value. The  $R_p$  values were also estimated by a fitting procedure assuming an appropriate equivalent electrical circuit (EEC) of the electrodes. As it is known, chromium significantly affects protective properties of the conversion layer: even a brief contact with air and/or aqueous media is sufficient to create a thin oxide layer on the electrode surface, which prevents further active chromium dissolution and penetration of the corrosive medium into the depth [25]. The passive oxide layer consists of an inner barrier layer and an outer precipitated oxide/hydroxide (porous) layer [26–28]. Usually the passive oxide systems are modelled by an equivalent electrical circuit (EEC) composed of two consecutive parallel (RC) sub-circuits in series with  $R_s$  (resistance of the solution layer between the reference electrode and the working one).  $C$  is the capacitance of the corresponding layer [29]. The EEC that accounts for the pure chromium behaviour in a borate solution was proposed by D. Marijan [30]. The EEC for the simulation of Cr and Cr + ZrO<sub>2</sub> coatings is shown in Fig. 8. The ECC for the Cr coating (Fig. 8a) composed of two (RC) sub-circuits corresponded to two overlapped capacitive loops at both medium and low frequencies. The resistance

of the passive layer, which consisted of Cr oxides, was taken into account. In this model, the resistance across the porous oxide layer and the constant phase element (CPE) are represented by  $R_{\text{por}}$  and  $CPE_{\text{por}}$  elements, respectively. The parallel combination of the second (RC) sub-circuit ( $R_{\text{ct}}$  and  $CPE_{\text{ct}}$  elements) is attributed to the charge transfer and Warburg impedance ( $W$ ), which represents diffusion limitations of the corrosion process [31]. The coded formula of this EEC is presented as  $R_s(CPE_{\text{por}}(R_{\text{por}}(CPE_{\text{ct}}(R_{\text{ct}}W))))$ . According to this EEC scheme, reactions occur only on the surface of the exposed electrode at the bottom of the pore, both  $R_{\text{por}}$  and  $R_{\text{ct}}$  affect the corrosion process and their sum corresponds to  $R_p$ . The CPE parameter is introduced in EEC instead of the pure capacitance  $C$  in order to accurately represent the surface heterogeneity [32, 31]. The impedance of the CPE element  $Z_{\text{CPE}}$  is defined by the ratio

$$Z_{\text{CPE}} = (j\omega)^{-n} Y_0^{-1}, \quad (2)$$

where  $Y_0$  is the electrode admittance,  $j$  is the imaginary number ( $j = (-1)^{1/2}$ ),  $\omega = 2\pi f$  is the angular frequency and  $n$  is a parameter which evaluates how far the interface was from the ideal capacitor ( $0 < n < 1$ ). The values 0, 0.5 and 1.0 of  $n$  indicate that the CPE of EEC behaves as if it were a pure resistor, the Warburg impedance and a capacitor, respectively. Furthermore, the Warburg impedance ( $W$ ) is located at the low frequency region to simulate the diffusion process taking place on/through the passive film.

In the cases of as deposited Cr + xZrO<sub>2</sub> coatings one more RC sub-circuit was added to the EEC (Fig. 8b). This new ( $R_1C_1$ ) pair reflected the influence of ZrO<sub>2</sub> particles incorporated into the porous layer ( $R_{\text{por}} CPE_{\text{por}}$ ). Both ECCs were characterized by the lowest chi square ( $\chi^2$ ) and weighing average error values. The fitted parameters of the corrosion process and those for the quality of simulation for all electrodes are presented in Tables 2 and 3. The standard error data and the  $\chi^2$  indicated a good fit of the spectra to EECs.

The EIS data provided more insight into the influence of ZrO<sub>2</sub> particles on the properties of the chromium coating. It can be seen that when the ZrO<sub>2</sub> particles were introduced

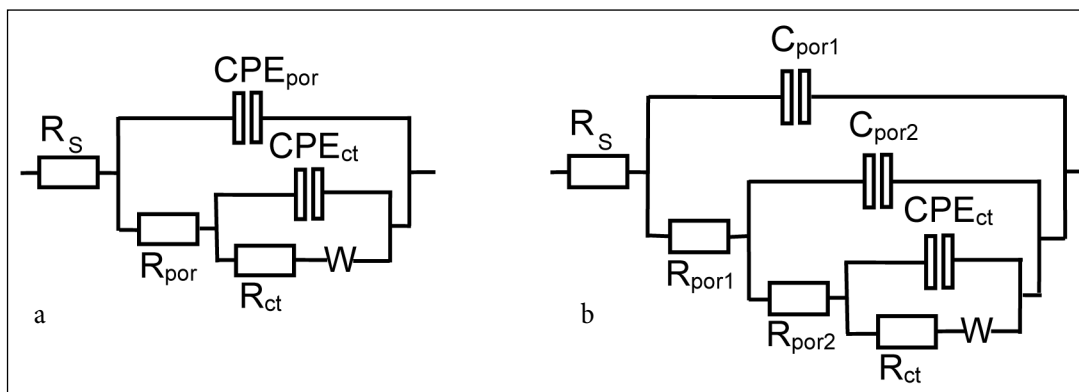


Fig. 8. Equivalent electrical circuit used for fitting of EIS data for deposited Cr (a) and Cr–ZrO<sub>2</sub> coating (b)

Table 2.  $R_s(CPE_{por}(R_{por}(CPE_{ct}(R_{ct}W))))$  equivalent circuit parameters determined by fitting impedance spectra for the as-deposited Cr coating immersed in a 3.5% NaCl solution

Sample	$R_s, \Omega \text{ cm}^2$	$CPE_{por} Ss^n \text{ cm}^{-2};$ (n)	$R_{por}, \Omega \text{ cm}^2$	$CPE_{ct} Ss^n \text{ cm}^{-2};$ (n)	$R_{ct}, \Omega \text{ cm}^2$	$W, S \text{ sec}^{-0.5} \text{ cm}^{-2}$	$\chi^2 (Z_{err}, \%)$
Cr	11.7	$47.7 \cdot 10^{-6}$ (0.84)	2929	$52.5 \cdot 10^{-6}$ (0.63)	19050	0.0019	$6.22 \cdot 10^{-5}$ (<0.78)

Table 3.  $R_s(C_{por1}(R_{por1}(C_{por2}(R_{por2}(CPE_{ct}(R_{ct}W))))))$  equivalent circuit parameters determined by modelling impedance spectra for the as-deposited Cr + ZrO<sub>2</sub> coatings immersed in a 3.5% NaCl solution

Sample	$R_s, \Omega \text{ cm}^2$	$C_{por1}, \mu\text{F cm}^{-2}$	$R_{por1}, \Omega \text{ cm}^2$	$C_{por2}, \mu\text{F cm}^{-2}$	$R_{por2}, \Omega \text{ cm}^2$	$CPE_{ct} Ss^n \text{ cm}^{-2}$ (n)	$R_{ct}, \Omega \text{ cm}^2$	$W, S \text{ sec}^{-0.5} \text{ cm}^{-2}$	$\chi^2 (Z_{err}, \%)$
Cr + 2 g l <sup>-1</sup> ZrO <sub>2</sub>	11.0	39.5	11.21	36.6	53.61	$26.28 \cdot 10^{-5}$ (0.71)	19360	0.002	$1.08 \cdot 10^{-4}$ (<1.04)
Cr + 6 g l <sup>-1</sup> ZrO <sub>2</sub>	9.3	54.7	6.84	88.3	23.8	$35.24 \cdot 10^{-5}$ (0.81)	10500	0.0016	$1.15 \cdot 10^{-4}$ (<1.07)
Cr + 10 g l <sup>-1</sup> ZrO <sub>2</sub>	10.5	66.6	4.88	120.1	20.55	$41.68 \cdot 10^{-5}$ (0.82)	20830	0.0004	$1.41 \cdot 10^{-4}$ (<1.19)

into the Cr coating, the resistance of the porous layer  $R_{por}$  was considerably reduced: from  $\sim 2929 \Omega \text{ cm}^2$  to  $\sim 63 \Omega \text{ cm}^2$  for Cr + 2 g l<sup>-1</sup> ZrO<sub>2</sub> (the last value could be roughly described as the sum of  $R_{por1}$  and  $R_{por2}$ ). It should be noted that the increase in the ZrO<sub>2</sub> content led to a decrease in  $R_{por}$ . According to the fitting data the overall capacitance of the porous layer increased when ZrO<sub>2</sub> particles were added to the chromium coating. The value of the  $R_{ct}$  was less influenced by addition of the ZrO<sub>2</sub> particles:  $R_{ct}$  negligibly increased for the Cr + 2 g l<sup>-1</sup> ZrO<sub>2</sub> and Cr + 10 g l<sup>-1</sup> ZrO<sub>2</sub> electrodes (Tables 2, 3). While for the Cr + 6 g l<sup>-1</sup> ZrO<sub>2</sub> electrode the decrease in  $R_{ct}$  from  $\sim 19050 \Omega \text{ cm}^2$  to  $\sim 10500 \Omega \text{ cm}^2$  was calculated. It can be presumed that changes in corrosion kinetics were determined by deterioration of the structure of the chromium coating. The introduction of ZrO<sub>2</sub> particles to the chromium coating led to a decrease in corrosion resistance.

It is of interest to consider how the concentration of ZrO<sub>2</sub> particles in the Cr(III) plating electrolyte affects the electrochemical properties of the Cr–ZrO<sub>2</sub> coating. For this purpose from the SEM images (Fig. 2) using the Image J 1.51n software (National Institute of Health, USA), part of the composite Cr–ZrO<sub>2</sub> surface area taken by the ZrO<sub>2</sub> particles has been determined. Measurements have revealed that ZrO<sub>2</sub> particles take 1/8, 1/7 or 1/5 of the composite Cr–ZrO<sub>2</sub> surface area when the ZrO<sub>2</sub> concentration in the chrome plating electrolyte (g l<sup>-1</sup>) is 2, 6 or 10, respectively. These results correlate well with the results obtained with the EDS method (Fig. 1). However, a higher surface area of the Cr–ZrO<sub>2</sub> composite taken by the ZrO<sub>2</sub> particles suggests a higher corrosion resistance of the composite (Fig. 2b–d), inasmuch as ZrO<sub>2</sub> particles should act as a barrier. Unfortunately, as our results obtained earlier have shown (Fig. 5–7), this is not the case. To explain this

phenomenon we propose a possible model of corrosion medium penetration ways through the Cr (Fig. 9a) and Cr–ZrO<sub>2</sub>

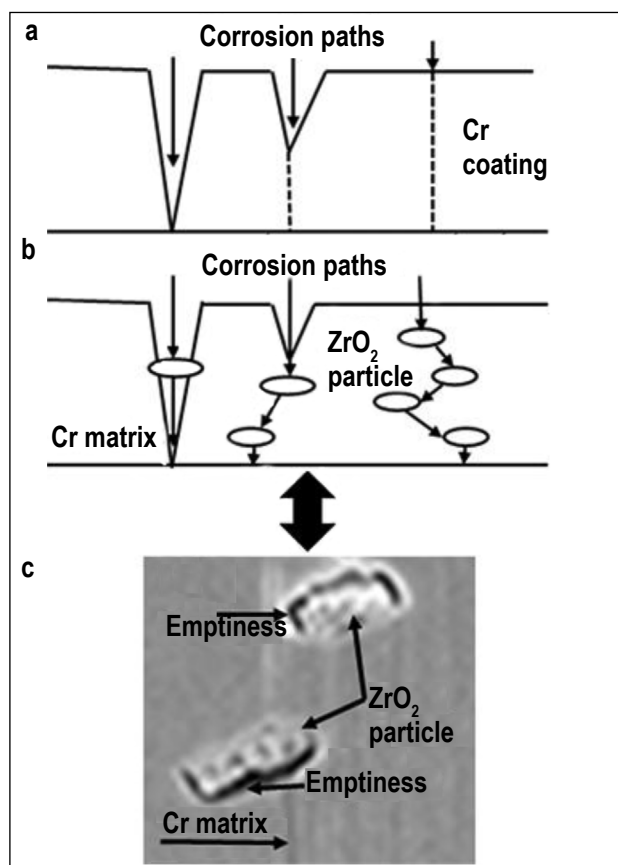


Fig. 9. A schematic illustration of the corrosion paths: (a) Cr coating without ZrO<sub>2</sub> particles, (b) with ZrO<sub>2</sub> particles and (c) photo of ZrO<sub>2</sub> in the Cr matrix

coatings (Fig. 9b). It is our opinion that the weak bonding between  $ZrO_2$  particles and the Cr matrix (Fig. 9c) increases further the number of already existing defects (Fig. 9a).

## CONCLUSIONS

Cr– $ZrO_2$  composites have been successfully deposited on Cu by DC electrodeposition. The main conclusions are as follows:

1. For the first time by applying the electrochemical DC method  $ZrO_2$  particles were incorporated into the Cr matrix obtained from the Cr(III) bath.

2. The increase in  $ZrO_2$  concentration in the Cr(III) electrolyte from 2 to 10 g l<sup>-1</sup> results in an increase in  $ZrO_2$  particles content in the Cr coating.

3. The surface microhardness (HV) of Cr– $ZrO_2$  composite coatings deteriorates with an increase in  $ZrO_2$  particles concentration in the Cr(III) electrolyte from 2 to 10 g l<sup>-1</sup>.

4.  $ZrO_2$  particles are distributed uniformly in the body of the Cr matrix deposited in the Cr(III) bath.

5. The electrochemical tests revealed that the corrosion resistance of Cr– $ZrO_2$  composites compared with the Cr coating is less. This was explained by a weak bonding between  $ZrO_2$  particles and Cr matrix.

Received 9 January 2018

Accepted 27 March 2018

## References

1. A. Hovestad, L. J. Janssen, *J. Appl. Electrochem.*, **25**, 519 (1995).
2. J. Li, C. S. Dai, D. L. Wang, X. G. Hu, *Surf. Coat. Technol.*, **91**, 131 (1997).
3. A. Banu, G. Carac, O. Radovici, M. Marcu, *Nonconv. Technol. Rev.*, **4**, 39 (2008).
4. R. Arghavani, N. Parvini-Ahmadi, *Surf. Eng.*, **27**, 649 (2011).
5. R. Arghavani, N. Parvini Ahmadi, S. Yazdi, B. Bosti, *Surf. Eng.*, **28**, 508 (2012).
6. S. Ramalingam, K. Balakrishnan, A. Subramania, *Trans. Inst. Met. Finish.*, **93**, 262 (2015).
7. K. Vathsala, T. Venkatarangiah Venkatesha, *Appl. Surf. Sci.*, **257**, 8929 (2011).
8. L. Benea, P. Ponthiaux, F. Wenger, *Surf. Coat. Technol.*, **205**, 5379 (2011).
9. S. Surviliene, A. Lisowska-Oleksiak, A. Češūnienė, *Corros. Sci.*, **50**, 338 (2008).
10. K. Hashimoto, K. Sugio, G. Sasaki, A. R. Setiawan, A. Ramelan, *Mech. Eng. J.*, **3**, 15-00623 (2016). DOI: 10.1299/mej.15-00623.
11. S. Lakra, H. S. Maharana, A. Basu, *Mater. Manuf. Processes*, **31**(11), 1447 (2016).
12. O. Sancakoglu, M. Erol, B. Agaday, E. Celik, *Mater. Technol.*, **47**(2), 601 (2013).
13. Z. X. Zeng, J. Y. Zhang, *Surf. Coat. Technol.*, **202**, 2725 (2008).
14. J. Gao, J. Suo, *Appl. Surf. Sci.*, **257**, 9643 (2011).
15. Z. Zeng, Y. Yu, J. Zhang, *J. Electrochem. Soc.*, **156**(4), C123 (2009).
16. G. Bikulčius, A. Češūnienė, A. Selskienė, V. Pakštas, T. Matijošius, *Surf. Coat. Tech.*, **315**, 130 (2017).
17. H. Simunkova, P. Pessenda-Garcia, J. Wosik, P. Angerer, H. Kronberger, G. E. Nauer, *Surf. Coat. Technol.*, **203**, 1806 (2009).
18. J. M. Huang, Y. Li, G. F. Zhang, X. D. Hou, D. W. Deng, *Surf. Eng.*, **29**, 194 (2013).
19. Salah-ud Din, A. Kaleem, *Mater. Chem. Phys.*, **53**, 48 (1998).
20. C. D. Wagner, W. M. Riggs, L. E. Davis, J. F. Moulder, G. E. Muilenberg, *Handbook of X-ray Photoelectron Spectroscopy*, p. 190, Perkin-Elmer, Minneapolis, MN (1978).
21. C. D. Wagner, A. V. Naumkin, A. Kraut-Vass, J. W. Allison, C. J. Powell, J. R. Rumble Jr., *NIST Standard Reference Database 20*, Version 3.4 (Web Version).
22. J. H. O. J. Wijenberg, M. Steegh, M. P. Aarnts, K. R. Lammers, J. M. C. Mol, *Electrochim. Acta*, **173**, 819 (2015).
23. A. J. Bard, L. R. Faulkner, *Electrochemical Methods, Fundamentals and Applications*, John Wiley & Sons, New York (2001).
24. P. Agarwal, M. E. Orazem, L. H. Garcia-Rubio, *J. Electrochem. Soc.*, **139**, 1917 (1992).
25. J. A. L. Dobbelaar, J. H. W. de Wit, *J. Electrochem. Soc.*, **137**(7), 2038 (1990).
26. D. D. Macdonald, *J. Electrochem. Soc.*, **139**, 3434 (1992).
27. D. D. Macdonald, A. Sun, N. Priyantha, P. Jayaweera, *J. Electroanal. Chem.*, **572**, 421 (2004).
28. J. Ai, Y. Chen, M. Urquidi-Macdonald, D. D. Macdonald, *J. Electrochem. Soc.*, **154**, C43 (2007).
29. L. Sziraki, E. Kuzmann, K. Papp, C. U. Chisholm, M. R. El-Sharif, K. Havancsak, *Mater. Chem. Phys.*, **133**, 1092 (2012).
30. D. Marijan, M. Gojic, *J. Appl. Electrochem.*, **32**, 1341 (2002).
31. V. F. Lvovich, *Impedance Spectroscopy*, New Jersey, John Wiley & Sons (2012).
32. U. Rammelt, G. Reinhard, *Electrochim. Acta*, **35**, 1045 (1990).
33. J. B. Jorcin, M. E. Orazem, N. Pabere, B. Tribollet, *Electrochim. Acta*, **51**, 1473 (2006).

G. Bikulčius, A. Češūnienė, A. Selskienė, A. Grigučevičienė, V. Jasulaitienė, M. Ger

## ELEKTROCHEMIŠKAI NUSODINTŲ Cr– $ZrO_2$ KOMPOZICINIŲ DANGŲ IŠ Cr(III) VONIOS APIBŪDINIMAS

### Santrauka

Darbo tikslas buvo elektrochemiškai nusodinti Cr– $ZrO_2$  kompozicines dangas iš Cr(III) vonios naudojant nuolatinę elektros srovę ir ištirti šių dangų apsaugines savybes. Dangos buvo formuojamos iš sulfatinio Cr(III) elektrolito, turinčio formiato ir urėjos junginių kaip kompleksodarių. Dangų skersinio šlifo tyrimai rodo, kad  $ZrO_2$  dalelės įsiterpia į Cr matricą ir yra tolygiai joje pasiskirsčiusios. Nustatyta, kad  $ZrO_2$  dalelės veikia Cr– $ZrO_2$  kompozicines dangas, gautos iš Cr(III) vonios, mikrokietumą, morfologiją ir korozinę elgseną.

